Inorganic Chemistry

Article

pubs.acs.org/IC

Hierarchy of Pyrophosphate-Functionalized Uranyl Peroxide Nanocluster Synthesis

Mateusz Dembowski,[†] Christopher A. Colla,[‡] Sarah Hickam,[§] Anna F. Oliveri,[∥] Jennifer E. S. Szymanowski,[§] Allen G. Oliver,[†] William H. Casey,[‡,∥] and Peter C. Burns*[,†,§]

[†]Department of Chemistry and Biochemistry and [§]Department of Civil and Environmental Engineering and Earth Sciences, University of Notre Dame, Notre Dame, Indiana 46556, United States

[‡]Department of Earth and Planetary Sciences and [∥]Department of Chemistry, University of California, Davis, California 95616, United States

Supporting Information

ABSTRACT: Herein, we report a new salt of a pyrophosphate-functionalized uranyl peroxide nanocluster $\{U_{24}Pp_{12}\}$ (**1**) exhibiting O_h molecular symmetry both in the solid and solution. Study of the system yielding **1** across a wide range of pH by single-crystal X-ray diffraction, small-angle X-ray scattering, and a combination of traditional ^{31}P and diffusion-ordered spectroscopy (DOSY) NMR affords unprecedented insight into the amphoteric chemistry of this uranyl peroxide system. Key results include formation of a rare binary $\{U_{24}\}$·$\{U_{24}Pp_{12}\}$ (**3**) system observed under alkaline conditions, and evidence of acid-promoted decomposition of $\{U_{24}Pp_{12}\}$ (**1**) followed by spatial rearrangement and condensation of $\{U_4\}$ building blocks into the $\{U_{32}Pp_{16}\}$ (**2**) cluster. Furthermore, ^{31}P DOSY NMR measurements performed on saturated solutions containing crystalline $\{U_{32}Pp_{16}\}$ show only trace amounts (~2% relative abundance) of the intact form of this cluster, suggesting a complex interconversion of $\{U_{24}Pp_{12}\}$, $\{U_{32}Pp_{16}\}$, and $\{U_4Pp_{4-x}\}$ ions.

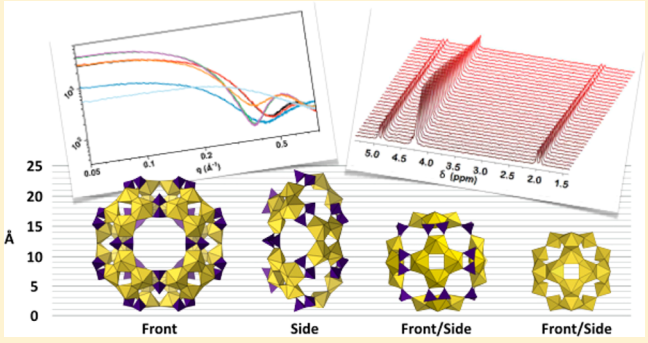

INTRODUCTION

Metal-oxide clusters are a group of discrete, macromolecular materials with potential applications in diverse fields such as single-molecule catalysis, surface chemistry, and biology.[1−4] The advancement of this field, driven by nearly two centuries of scientific exploration, resulted in the description of structures ranging from simple Lindqvist, Keggin, and Dawson types to exotic sphere-, wheel-, and hedgehog-shaped polyoxometalates (POMs).[5−8] Consequently, examination of these systems provided grounds for development of structure−property relationships and design of task-specific molecules.[9−13] Actinide peroxide nanoclusters represent a relatively new subclass of POMs that are interesting due to their importance in advanced nuclear fuel cycles and for understanding the environmental mobility of actinides.[14,15] Their finite and nanoscale nature provides unique opportunities for development and validation of computational models used in the fields of geo- and actinide chemistry.[16−20] Extreme radiation fields, such as those present during a nuclear reactor failure, can potentially lead to formation of sufficient amounts of peroxide (via α-radiolysis of water) to support self-assembly of actinide peroxide nanoclusters.[21,22] Since their discovery in 2005, more than 60 unique actinide peroxide nanoclusters have been published.[23,24]

These discrete, hollow, and negatively charged species form readily under ambient aqueous conditions and across a wide range of pH conditions.[24] The identity, size, and charge of the resulting species depends on the choice of functional group and counterion used in the synthesis.[25,26]

The details of the solution chemistry of uranyl peroxide nanoclusters, including the mechanism of self-assembly, remain limited.[27−30] A subclass of uranyl peroxide nanoclusters containing pyrophosphate (Pp) bridges between uranyl ions offers a unique opportunity to explore their solution chemistry prior, and subsequent to, their crystallization via nuclear magnetic resonance (NMR) spectroscopy (^{31}P s = 1/2, γ = 17.25 MHz/tesla).[31] A significant advantage of this technique, as compared to electrospray ionization mass spectrometry (ESI-MS) or small-angle X-ray scattering (SAXS), is the simultaneous detection of all NMR active species irrespective of their size, charge, or shape. Initial efforts afforded insights into the energetics of conformational changes of the Na/K salt of $\{U_{24}Pp_{12}\}$ and the acid-catalyzed nature of its formation.[27,32] DOSY NMR studies of transition-metal POMs and uranyl peroxide nanoclusters containing pyrophosphate or phosphonic bridges allowed unequivocal assignment of signals observed in traditional NMR spectra to specific cluster species by determining their hydrodynamic radii.[32−35] Herein we use the

Received: March 15, 2017
Published: April 10, 2017

DOI: 10.1021/acs.inorgchem.7b00649
Inorg. Chem. 2017, 56, 5478−5487

potential of DOSY in conjunction with traditional NMR and SAXS measurements to provide insight into the chemistry of the uranium−peroxide−pyrophosphate system across a range of pH conditions.

EXPERIMENTAL SECTION

Warning! *Uranium-238 is a weak α-emitter (α = 4.467 MeV). All experiments described herein were conducted by trained personnel in laboratories equipped and licensed to work with radioactive elements.*

General Considerations. Uranyl nitrate hexahydrate ($UO_2(NO_3)_2{\cdot}6H_2O$, International Bio-Analytical Industries, Inc.), hydrogen peroxide (30% aqueous solution, EMD Millipore), sodium pyrophosphate ($Na_4P_2O_7$, Spectrum), oxalic acid ($H_2C_2O_4$, Sigma-Aldrich), lithium hydroxide (LiOH, EMD Millipore), and deuterium oxide (D_2O, Cambridge Isotope Laboratories, Inc.) were obtained from commercial suppliers and used without further purification. Pyrophosphate functionalized uranyl peroxide nanoclusters are abbreviated as $\{U_nPp_m\}$, where n corresponds to the number of $[(UO_2)(O_2)]$ units, and m gives the number of bis-bidentate pyrophosphate ($P_2O_7^{4-}$, Pp) bridges. Nonfunctionalized nanoclusters are designated $\{U_n\}$, where n is the number of $[(UO_2)(O_2)(OH)^-]$ units. The syntheses of Li/Na salts of $\{U_{24}Pp_{12}\}$ (**1**), $\{U_{32}Pp_{16}\}$ (**2**), and $\{U_{24}\}{\cdot}\{U_{24}Pp_{12}\}$ (**3**) were realized according to previously described procedures[27] by substituting tetraethylammonium hydroxide ($N(CH_2CH_3)_4OH$, TEAOH) and iodic acid (HIO_3) for lithium hydroxide (LiOH) and oxalic acid ($H_2C_2O_4$), respectively. Crystals of (**2**) and (**3**) were obtained from the same stock solution as (**1**) by adjusting the pH conditions to favor their formation. Tables 1 and S1 list the specific pH conditions that led to crystallization of all studied structures. It was earlier noted that the presence of potassium and iodate (IO_3^-) in the Na/K salt of $\{U_{24}Pp_{12}\}$ resulted from contamination of TEAOH, and that iodate was added.[27] To obtain a pure Li/Na salt of $\{U_{24}Pp_{12}\}$ both reagents were eliminated.

Table 1. Crystallographic Data for Primary Unit Cells of $\{U_{24}Pp_{12}\}$, $\{U_{32}Pp_{16}\}$, and $\{U_{24}\}{\cdot}\{U_{24}Pp_{12}\}$

compound	**1a**	**2a**	**3**
empirical formula	$U_{24}P_{24}O_{180}$	$U_{32}P_{32}O_{224}$	$U_{48}P_{24}O_{108}$
molecular weight [g mol^{-1}]	9335.96	12 191.95	13 896.69
crystal system	triclinic	orthorhombic	tetragonal
space group	$P\bar{1}$	*Imm*2	*P*4/*mbm*
a [Å]	20.868(3)	28.516(3)	31.607(3)
b [Å]	20.964(3)	28.524(3)	31.607(3)
c [Å]	21.200(3)	28.416(3)	22.707(2)
α [Å]	107.4243(19)	90	90
β [Å]	106.9382(19)	90	90
γ [Å]	113.2611(18)	90	90
V [Å^3]	7187.6(18)	23 114(5)	22 685(5)
Z	1	2	2
R_1/wR_2 [for $I > 2\sigma(I)$]	0.0800/0.1724	0.0571/0.1555	0.0436/0.1113
R_1/wR_2 [for all data]	0.1063/0.1820	0.0768/0.1736	0.0673/0.1271
GOF	1.161	1.070	1.077
largest diff. peak/hole [e Å^{-3}]	4.52/−3.10	3.21/−1.72	3.39/−2.88
pH observed	7	5, 6	9, 10
approximate Li/Na ratio	1:1	1:1	1.3:1

Variation of pH. Combining 10 mL of 0.5 M $UO_2(NO_3)_2$, 10 mL of 30% H_2O_2, and 12.5 mL of 0.2 M $Na_4P_2O_7$ in a 50 mL beaker results in rapid precipitation of *studtite*, $[(UO_2)(O_2)(H_2O)_2]{\cdot}2H_2O$.[36] Titration of the resulting suspension using 2.38 M LiOH results in gradual dissolution of the solid accompanied by effervescence and a color change to dark orange (pH = 9.3). Aliquots (5 mL) of the resultant solution were transferred into 20 mL scintillation vials, and their pH was adjusted over time to target values using 0.01−0.5 M $H_2C_2O_4$ and/or 0.1−2.38 M LiOH (see Supporting Information).

Single-Crystal X-ray Diffraction. Crystals suitable for X-ray diffraction were transferred into oil from their mother solutions and mounted on cryoloops. Data collections were performed under a stream of nitrogen gas, affording a temperature of 100 K. A full sphere of data was collected for each crystal using a Bruker APEX II Quazar diffractometer (microsource sealed tube with multilayer monochromated Mo Kα X-rays) using frame widths of 0.5° in ω and an exposure time of 10−60 s. Data integrations, including corrections for Lorentz, polarization, and background effects, were performed using the Bruker APEX III software. Absorption corrections were applied using SADABS.[37] SHELXTL[38,39] was used for structure solution and refinement. Positions of H atoms were not located in the structure. Crystallographic information is summarized in Tables 1 and S1. The structure of the Li/Na $\{U_{32}Pp_{16}\}$ (**2a**) was refined as an inversion twin with a ratio of 0.570:0.430 indicating a racemic mixture.

NMR Measurements. One-dimensional (1D) ^{31}P NMR spectra were recorded using a 500 MHz Varian INOVA spectrometer (11.57 T) with 56 dB power level attenuation, 14.8 ms pulse length, 5 s relaxation delay (d1), and 124 scans. Diffusion-ordered spectroscopy data (DOSY) were recorded using a 500 MHz Bruker AVANCE DRX spectrometer (11.74T), equipped with a Bruker BBO 5 mm probe. DOSY data were collected using the stimulated echo stegp1s two-dimensional (2D) pulse sequence for pulsed field-gradient measurements. Data were acquired by varying the diffusion gradient lengths (δ) from 1 to 2 s and the diffusion delay times (Δ) from 2000 to 3000 μs.

Prior to NMR measurements, reaction mixtures were pH-adjusted using $H_2C_2O_4$ and/or LiOH and aged until a steady state was achieved (see Supporting Information). All reaction mixture measurements were performed in the presence of a D_2O insert that allowed for signal locking and shimming. ^{31}P NMR chemical shifts are reported with respect to neat H_3PO_4. Standard samples used in 1D ^{31}P as well as DOSY NMR studies were prepared by dissolution of 15 mg of **1** (or **2**) in 1 mL of deuterium oxide.

Small-Angle X-ray Scattering (SAXS). Measurements of X-ray scattering for reaction mixtures (pH = 4−10) and standard solutions were performed on a Bruker Nanostar equipped with a Montel multilayer optics and HiSTAR multiwire detector and radiation provided from a Cu microfocus source. Standard solutions were prepared by dissolution of 15 mg of **1** (or **2**) in 1 mL of ultrapure water. Sample solutions were introduced into the instrument through a flow cell located 26.3 cm from the detector followed by 2 h of data collection. Blank solutions containing the solvent (H_2O) were examined using the same procedures for measurement of the background effects. Experimental data were fitted using the Irena SAS package as implemented in Igor Pro software.[40]

Characterization Data. Additional crystallographic data are available in Table S1 and in CIF format. Raman spectra of **1**, **2**, and **3** with peak assignments are available in Figure S1. ESI-MS results are available in Figure S2 and Table S2. TGA results are summarized in Figures S3−S5. Elemental analysis results (ICP-OES) are summarized in Table S3.

RESULTS AND DISCUSSION

Description of Cluster Topologies, Symmetries, and Their NMR Signatures. $Li_{48-x}Na_x[(UO_2)_{24}(O_2)_{24}(P_2O_7)_{12}]{\cdot}nH_2O$, (**1**) ($x \approx 24$ for **1a** and **1b**, $x \approx 12$ for **1c**, $n \approx 120$). The Li/Na salt of $\{U_{24}Pp_{12}\}$ crystallizes, depending on the pH, in three unique triclinic, $P\bar{1}$ (No. 2) unit cells. The structure of the anion consists of 24 uranyl polyhedra arranged into six uranyl peroxide tetramers $[(UO_2)_4(O_2)_4]$, $\{U_4\}$ internally bridged via $\mu{:}\eta^2{-}\eta^2$ peroxide $[O_2^{2-}]$ ligands and externally cross-linked via 12 bis-bidentate pyrophosphate (Pp) bridges, resulting in hollow, negatively charged (−48) molecules with idealized O_h symmetry (Figure 1). Charge balance is afforded by combinations of hydrated Li and Na ions located inside of

DOI: 10.1021/acs.inorgchem.7b00649
Inorg. Chem. 2017, 56, 5478−5487

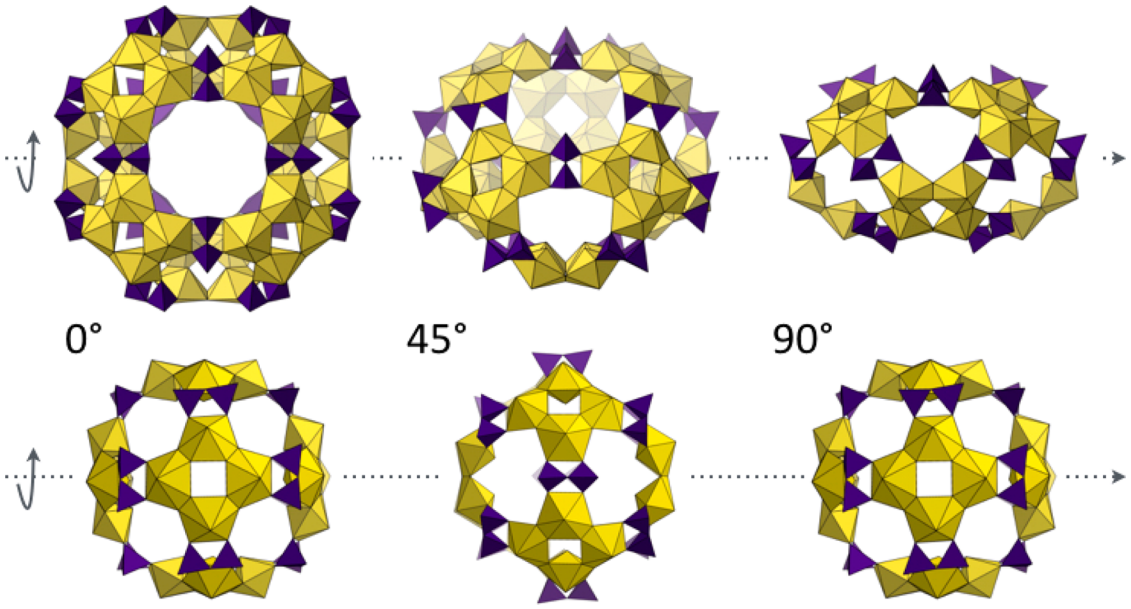

Figure 1. Polyhedral representation of the Li/Na salts of $\{U_{32}Pp_{16}\}$ (top) and $\{U_{24}Pp_{12}\}$ (bottom). Uranyl and phosphate polyhedra are shown in yellow and purple, respectively.

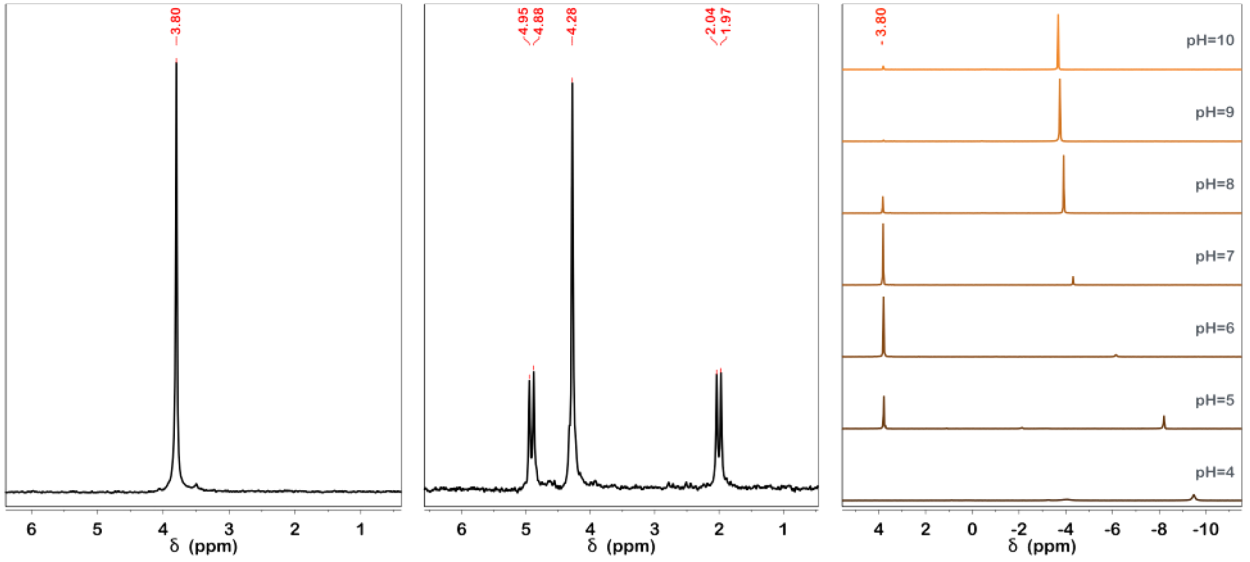

Figure 2. ^{31}P NMR of $\{U_{24}Pp_{12}\}$ (left), $\{U_{32}Pp_{16}\}$ (center), and reaction mixtures containing stoichiometric amounts of uranium and pyropshosphate (right).

the nanocluster, as well as in the interstitial space. The molecular dimensions of the $\{U_{24}Pp_{12}\}$ anion, as defined by the distance between the centers of terminal oxygen atoms in **1a**, are 1.78 × 1.77 × 1.76 nm^3 (ellipticity, e = 0.15, see Supporting Information). The average uranyl (U−O_{yl}), peroxide (O−O), uranium-peroxide (U−O_{per}), and uranium-pyrophosphate (U−O_{Pp}) bond lengths are 1.791(12), 1.474(16), 2.371(40), and 2.397(17) Å, respectively. In accordance with its O_h symmetry, the Li/Na salt of $\{U_{24}Pp_{12}\}$ displays a single type of $\{U_4\}$ unit defined with respect to the center of mass of the cluster as convex and characterized by four ∼133° U−Pp−U dihedral angles. This result is noteworthy, because it agrees with previous hypothesis that the $\{U_{24}Pp_{12}\}$ anion, originally characterized as a mixed Na/K salt (D_{4h} molecular symmetry),[27] would assume a higher symmetry conformation (O_h) in the absence of potassium. ^{31}P NMR spectra obtained by dissolution of pure crystals of **1a** (**1b**, or **1c**) in ultrapure water yields a single signal located at 3.80 ppm, in agreement with the solid-state symmetry of the anion (Figure 2).

$Li_{68-x}Na_x[(UO_2)_{32}(O_2)_{32}(P_2O_7)_{16}]\cdot nH_2O$, (**2**) ($x \approx 34$, $n \approx 275$). The Li/Na salt of $\{U_{32}Pp_{16}\}$ crystallizes in monoclinic, $P2_1/m$ (No. 11), monoclinic, $C2/c$ (No. 15), and orthorhombic, $Imm2$ (No. 44) space groups. The previously reported[25] structure of the anion consists of 32 uranyl polyhedra arranged into eight uranyl peroxide tetramers $\{U_4\}$ cross-linked via 16 bis-bidentate Pp bridges, resulting in a hollow, negatively charged (−68), wheel-shaped molecule showing idealized D_{4d} symmetry (Figure 1). The charge balance of the system is afforded by a combination of hydrated Li and Na ions. The molecular dimensions of the $\{U_{32}Pp_{16}\}$ anion in **2a** are 2.46 × 2.46 × 1.32 nm^3 (e = 0.85). The average U−O_{yl}, O−O, U−O_{per}, and U−O_{Pp} bond lengths are

DOI: 10.1021/acs.inorgchem.7b00649
Inorg. Chem. 2017, 56, 5478−5487

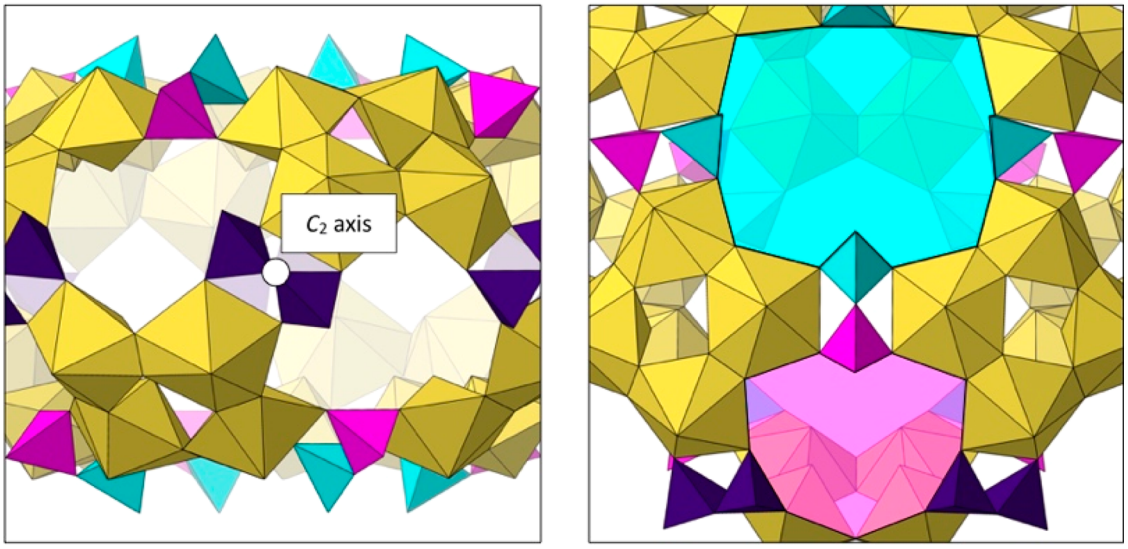

Figure 3. Polyhedral representation of the Li/Na salt of $\{U_{32}Pp_{16}\}$. (left) Pp bridges located in the equatorial region of the anion with the C_2 rotation axis passing through the P−O−P bridge. (right) Pp bridges located in the polar regions of the anion showing dissimilar chemical environment highlighted in magenta and teal. Yellow polyhedra represent uranium, and purple, magenta, and teal all represent phosphorus.

1.790(11), 1.475(19), 2.370(39), and 2.402(28) Å, respectively. The structure of $\{U_{32}Pp_{16}\}$ shows one type of $\{U_4\}$ unit (convex) characterized by two ∼125° and two ∼152° U−Pp−U dihedral angles distributed between the equatorial and polar regions of the anion, respectively. ^{31}P NMR spectra obtained by dissolution of pure crystals of **2a** (**2b** or **2c**) in ultrapure water yielded three signals located at 1.97/2.04 (d, $^2J_{P-P}$ = 13.7 Hz), 4.28 (s), and 4.88/4.95 (d, $^2J_{P-P}$ = 13.7 Hz) ppm, with a 1:2:1 ratio, successively (Figure 2). We assign the signal observed at 4.28 (s) ppm to the group of Pp bridges located in the equatorial region of the anion. This assignment is based on their ratio within the structure and the symmetry relation of the P atoms present within (Figure 3). The two doublets observed at 1.97/2.04 and 4.88/4.95 ppm are assigned to the Pp bridges located on the polar regions of the cluster. The signal splitting, J = 13.7 Hz, is comparable with previously reported values for ^{31}P−^{31}P spin−spin coupling[41,42] and is consistent with distinctive chemical environments that are experienced by individual P atoms present in these bridges (Figure 3).

$Li_{72-x}Na_x[(UO_2)_{24}(O_2)_{24}(OH)_{24}\cdot(UO_2)_{24}(O_2)_{24}(P_2O_7)_{12}]\cdot nH_2O$, **3** ($x \approx 31$, $n \approx 240$). The Li/Na salt of the binary $\{U_{24}\}\cdot\{U_{24}Pp_{12}\}$ cluster system crystallizes in the tetragonal $P4/mbm$ (No. 127) space group. Its crystal structure consists of 48 uranyl polyhedra arranged into 12 uranyl peroxide tetramers $\{U_4\}$, six of which are cross-linked via 24 μ−OH bridges resulting in a hollow, negatively charged (−24) $\{U_{24}\}$ cluster showing idealized O_h molecular symmetry (Figure 4). The molecular dimensions of the $\{U_{24}\}$ anion are 1.43 × 1.44 × 1.45 nm^3 (e = 0.16). The average U−O_{yl}, O−O, U−O_{per}, and U−OH bond lengths are 1.798(8), 1.483(3), 2.385(32), and 2.392(10) Å, respectively. The remaining six $\{U_4\}$ subunits are cross-linked via 12 bis-bidentate Pp bridges resulting in a hollow, negatively charged (−48) $\{U_{24}Pp_{12}\}$ cluster with idealized D_{4h} molecular symmetry (Figure 4). The molecular dimensions of the $\{U_{24}Pp_{12}\}$ anion are 1.43 × 1.83 × 1.84 nm^3 (e = 0.63). The average U−O_{yl}, O−O, U−O_{per}, and U−O_{Pp} bond lengths are 1.793(6), 1.479(6), 2.377(36), and 2.415(23) Å, respectively. Consistent with its D_{4h} molecular symmetry, the $\{U_{24}Pp_{12}\}$ anion present in this system displays two distinct types of $\{U_4\}$ units that are defined as convex (four units) or concave (eight units). Convex units are characterized by four ∼103° U−Pp−U dihedral angles and concave units by two ∼103° and two ∼141° U−Pp−U dihedral angles mirroring the previously reported Na/K salt.[27] Charge balance is afforded by a combination of hydrated Li and Na ions. ^{31}P NMR spectra obtained for a solution of **3** in ultrapure water yields two signals at 3.80 and −2.31 ppm with a 4.5:1 ratio, respectively (Figure S7). The signal observed at 3.80 ppm is assigned to the $\{U_{24}Pp_{12}\}$ anion in its O_h conformation, and that at −2.31 ppm is assigned to uncoordinated Pp, the presence of which is

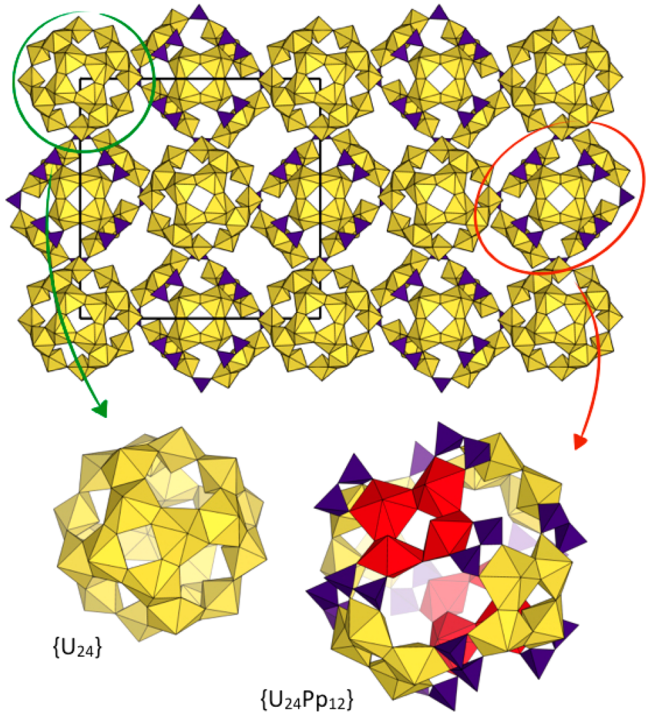

Figure 4. Polyhedral representation of the binary $\{U_{24}\}\cdot\{U_{24}Pp_{12}\}$ system. The idealized D_{4h} symmetry observed for the $\{U_{24}Pp_{12}\}$ is caused by two concave $\{U_4\}$ units (red polyhedra). Yellow and red polyhedra represent uranium; purple polyhedra represent phosphorus.

DOI: 10.1021/acs.inorgchem.7b00649
Inorg. Chem. 2017, 56, 5478−5487

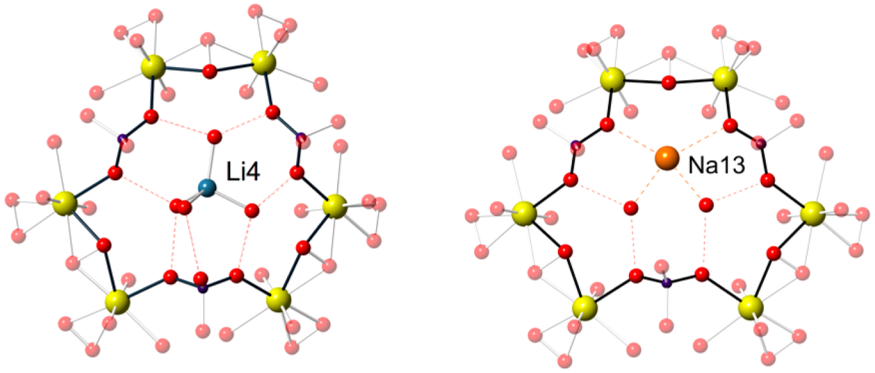

Figure 5. Ball-and-stick representation of the quasi-hexagonal pores present in the $\{U_{24}Pp_{12}\}$ anion. (left) Solvated Li tetrahedron present within the hexagonal pore of **2a**. (right) Sodium cation occupying the same pore space within the structure of **2b**. Yellow, purple, red, blue, and orange spheres represent uranium, phosphorus, oxygen, lithium, and sodium, respectively. Red and orange dashed lines represent H-bonds and strong ionic sodium−oxygen interactions.

attributed to partial decomposition of $\{U_{24}Pp_{12}\}$. Sample impurity of this magnitude is unlikely according to the results obtained via ICP-OES (see Supporting Information). This unique system demonstrates Pp bridge pliability, as it assumes a favorable lower-symmetry (D_{4h}) conformation in the solid state (increased packing efficiency) and higher O_h conformation upon dissolution. Similar conformer discrepancy (i.e., solid state vs solution) has been previously noted for phosphine functionalized uranyl peroxide nanoclusters.[33]

Multiplicity of Observed Unit Cells and Refinement of Cation Positions. Depending on the pH of the system, the size of the cation, and the strength of its interactions with the surface of the anion, specific cluster topologies can crystallize in various crystal systems, or in the same system with different unit cells. This behavior has been previously noted for the Li salt of the $\{U_{24}\}$ cluster.[29] Comparison of structures of $\{U_{24}Pp_{12}\}$ obtained in this study reveal that the pseudohexagonal pores are occupied either by Li (**1a**, Figure 5a) or Na cations (**1b**, Figure 5b). It is likely that the observed nonpreferential binding of lighter alkali metals to the surface of uranyl peroxide nanoclusters led to two Li/Na ratios observed for $\{U_{24}Pp_{12}\}$ systems (1:1 for pH = 7−8, and 3:1 for pH = 9). The cluster $\{U_{24}Pp_{12}\}$ crystallizes with Li and Na counter cations in two different ratios (one for **1a** and **1b** and another for **1c**). The ^{31}P NMR and Raman spectra of materials corresponding to the different cation ratios are indistinguishable, indicating that the identity of the cations is more important than their relative abundances. The solvent and cation-accessible voids within the unit cell of **1a** are estimated to be 4102 Å^3, or 57.1% (see Supporting Information). Because of the considerable void space noted for **1a**, some of the crystallographically determined cation positions, especially those of lighter elements, are probable rather than absolute positions within the structure. As such, implementation of partial occupancy treatment during the refinement of cation and solvent molecules was considered appropriate and consistent with the previously noted solid-state mobility of lighter alkali metals in the $\{U_{24}\}$ and $\{U_{28}\}$ systems.[43,44]

Solution Speciation. Characterization of species present in solution prior to crystallization was performed using a combination of SAXS and traditional ^{31}P NMR measurements. SAXS is an effective tool for in situ studies of nanocluster self-assembly.[28,29,45−49] Herein we implement ^{31}P NMR as a complementary characterization technique allowing for determination of all phosphorus-containing species irrespective of their size, charge, or shape. A summary of results observed via SAXS, ^{31}P NMR, and single-crystal X-ray diffraction measurements is presented in Figure 6.

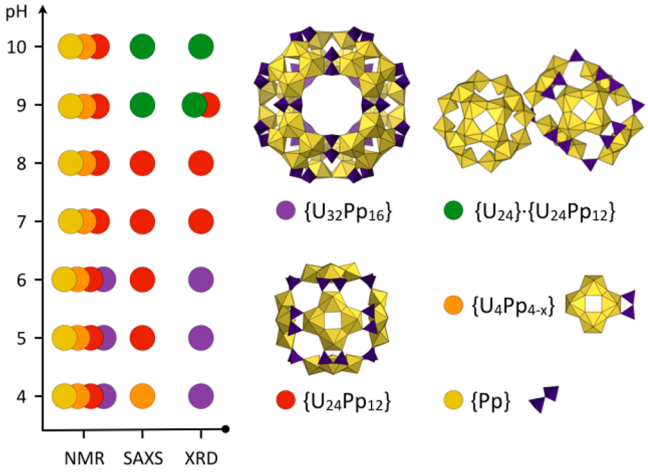

Figure 6. Schematic representation of the results obtained from solid-state (XRD) and solution mode (NMR, SAXS) measurements of systems containing stoichiometric amounts of uranium and pyrophosphate (U/Pp = 2:1) as a function of pH.

SAXS profiles for all but the pH = 4 system indicate the presence of hollow spherical nanoclusters (Figure 7). Guinier analysis of the low-q regions provides radii of gyration (R_g) ranging from 7.65 ± 0.05 to 9.01 ± 0.06 Å. The profile for solution with pH = 4 yields R_g = 3.86 ± 0.05 Å. A summary of the SAXS results is available in Supporting Information. For the solutions considered in this study, the value of R_g initially increases from 7.65 ± 0.05 Å (pH = 10) to 9.01 ± 0.06 Å (pH = 6) and consequently decreases to 8.32 ± 0.06 (pH = 5) and 3.86 ± 0.05 Å (pH = 4). The progressive, rather than immediate change of R_g across pH conditions suggests heterogeneity of the system and as such represents the average size of species present in solution. Co-crystallization of $\{U_{24}\}$·$\{U_{24}Pp_{12}\}$ provides evidence for simultaneous existence of two cluster species and corroborates the hypothesis of heterogeneous systems. Moreover, the statistical average of R_g obtained for $\{U_{24}\}$ and $\{U_{24}Pp_{12}\}$ using the Crysol software[50] (7.59 Å, see Supporting Information) is in good agreement with the values observed for the two solutions yielding the co-

DOI: 10.1021/acs.inorgchem.7b00649
Inorg. Chem. 2017, 56, 5478−5487

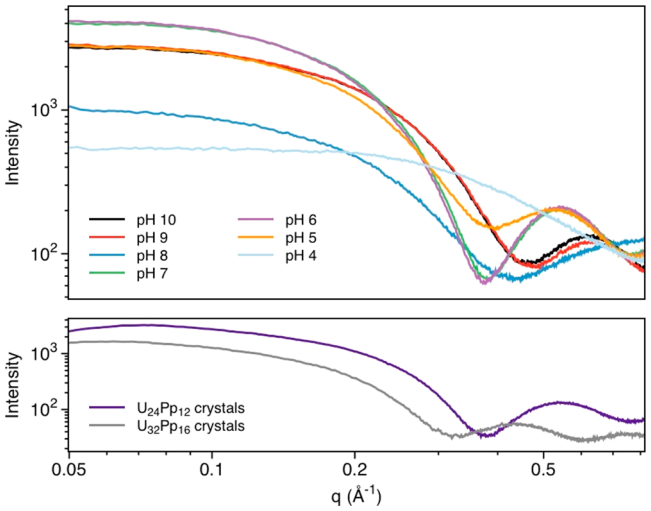

Figure 7. SAXS curves obtained from variable pH reaction mixtures (top) and crystals of $\{U_{24}Pp_{12}\}$ and $\{U_{32}Pp_{16}\}$ dissolved in ultrapure water (bottom).

crystallized system ($R_{g,10}$ = 7.65 ± 0.05 Å, $R_{g,9}$ = 7.87 ± 0.05 Å). Comparison of these R_g values with those obtained from dissolution of the binary system would be unreliable due to the partial decomposition of $\{U_{24}Pp_{12}\}$, as indicated by ^{31}P NMR spectra (see above). The increasing R_g, with maximum observed for solution at pH = 6 (9.01 ± 0.06 Å), may indicate preferential formation of $\{U_{24}Pp_{12}\}$ under acidic conditions.[27]

Overall, the pH-dependent change in R_g values of cluster-bearing solutions coupled with our ability to crystallize the Li/Na salt of $\{U_{24}Pp_{12}\}$ across a range of pH values (pH = 7–9) agree with its predicted R_g value of 8.44 Å and acid-promoted assembly. Unanticipated behavior occurred over the pH range from 4 to 6. While the Guinier analysis of scattering curves indicates the presence of $\{U_{24}Pp_{12}\}$ at pH = 5–6 and the absence of any cluster species at pH = 4, the only species observed in the crystalline form in that pH range is the Li/Na salt of $\{U_{32}Pp_{16}\}$. Similarly, comparison of SAXS curves obtained by dissolution of crystalline $\{U_{24}Pp_{12}\}$ and $\{U_{32}Pp_{16}\}$ with those obtained from reaction mixtures provides no evidence of $\{U_{32}Pp_{16}\}$ presence in solution (Figure 7), emphasizing the need for additional solution studies.

To further probe the complex system revealed by the SAXS studies, and to gain size-independent information about solution speciation, ^{31}P NMR spectra were collected for all pH-adjusted reaction mixtures containing stoichiometric amounts of uranium and pyrophosphate. Most spectra show that the pH of the solution affects the quantity of the $\{U_{24}Pp_{12}\}$ anion present in solution, with highest in situ determined yields (90.54%) observed at pH = 6 (δ = 3.8 ppm, Figure 2). The NMR spectra were not normalized. Line broadening of some signals (e.g., pH = 4) results in their relatively low intensity as compared to those for solutions at other pH values. NMR spectra showing positions of signals arising from the minor species are in the Supporting Information. The concentration of $\{U_{24}Pp_{12}\}$ in solution declines below pH = 6 in accordance with SAXS scattering profiles. This result illustrates the acid-promoted nature of $\{U_{24}Pp_{12}\}$ formation (up to pH = 6), as well as its limited pH stability (pH < 6). Contrary to the results noted for the Na/K salt of $\{U_{24}Pp_{12}\}$,[27] ^{31}P NMR spectra obtained from the Li/Na system show only two major signals, one of which corresponds to the intact cluster (δ = 3.8 ppm) and the other that is assigned to an uncoordinated pyrophosphate/small uranyl–peroxo pyrophosphate unit (δ = −3.67 to −9.47 ppm). The range of chemical shifts observed for the latter species is attributed to the progressive protonation of the pyrophosphate unit at lower pH.[51] These findings reveal preferential formation of $\{U_{24}Pp_{12}\}$ containing topological squares in systems containing early alkali metals in agreement with trends predicted by density functional theory.[26,52] The lack of other major signals in the ^{31}P NMR spectra indicates the ephemeral and reactive nature of intermediates such as a pyrophosphate bound tetramer $\{U_4Pp_{4-x}\}$ (x = 1–3). Because

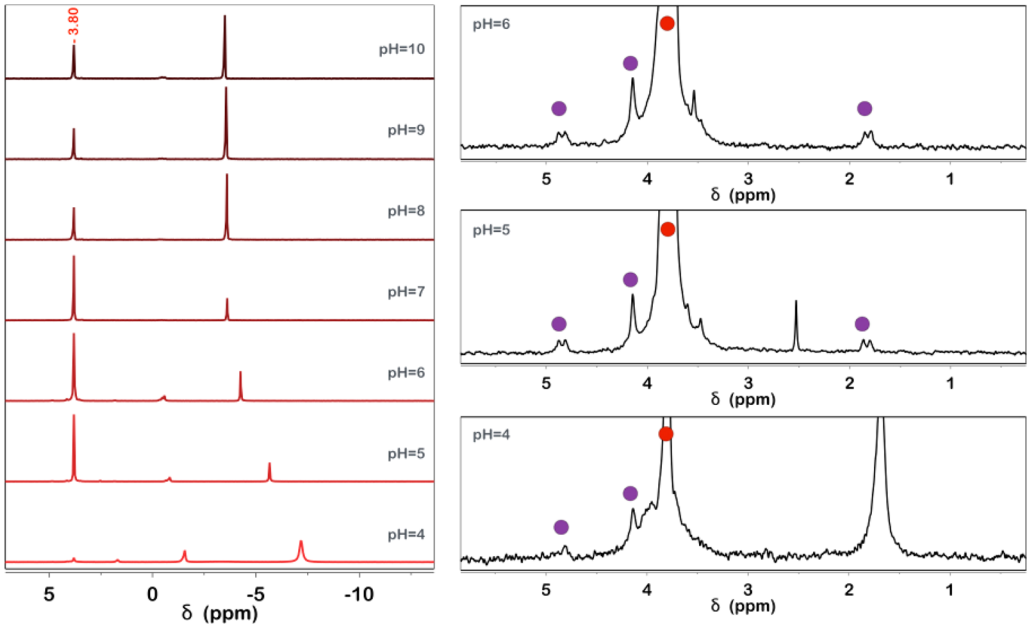

Figure 8. ^{31}P NMR spectra of saturated systems (left) and detailed view of saturated systems at pH = 4–6 with signals corresponding to $\{U_{24}Pp_{12}\}$ and $\{U_{32}Pp_{16}\}$ anions indicated in red and purple circles, respectively.

DOI: 10.1021/acs.inorgchem.7b00649
Inorg. Chem. 2017, 56, 5478–5487

of a lack of NMR-active nuclei within the basic uranyl peroxide building blocks, it is difficult to identify their specific roles in the formation of $\{U_{24}Pp_{12}\}$ and/or $\{U_{32}Pp_{16}\}$.

Further inspection of ^{31}P NMR spectra for uranyl peroxide solutions reveals signals between −0.41 ppm (pH = 9) and −4.05 ppm (pH = 4) present at low intensity under most pH conditions (pH = 5 to 10), with these becoming a major species only at pH = 4. Akin to the uncoordinated/small uranyl peroxide pyrophosphate species, the range of observed chemical shifts shows a strong dependence on the pH of the system, likely due to progressive protonation of the associated Pp units. We assign the signals in that chemical shift range to the coordinated uranyl peroxide tetramer unit $\{U_4Pp_{4-x}\}$ based on its relatively low abundance in systems displaying intact clusters and significant peak broadening (pH = 10, −0.56 ppm, full width at half-maximum (fwhm) = 28.49 Hz). The R_g obtained from the Guinier analysis of the X-ray scattering curve at pH = 4 (3.86 ± 0.05 Å) is in accord with the calculated R_g for an isolated $\{U_4\}$ unit (3.91 Å, see Supporting Information). This result, paired with severe broadening of ^{31}P NMR signals observed at −3.26 (fwhm = 30.08 Hz) and −4.05 ppm (fwhm = 81.86 Hz) at pH = 4 (see Figure S8), suggests a complex interconversion between $\{U_4Pp_{4-x}\}$ units.

SAXS curves and 1D ^{31}P NMR spectra obtained from reaction mixtures do not indicate the presence of the $\{U_{32}Pp_{16}\}$ anion in any of the examined solutions. This result is unexpected, because most actinyl peroxide nanoclusters have been shown to assemble in solution within hours to days,[29,53−55] although formation of more complex structures may require more time.[28,56] For instance, a time-resolved study of the self-assembly of a hybrid uranium-transition-metal cluster indicated that prior to the formation of the final products, other nanosized objects assembled and subsequently dissociated in the reaction mixture.[28] In a study of studtite dissolution, the initial species was identified as $\{U_{28}\}$, which over time gradually reacted to yield $\{U_{24}\}$ as the final product.[29]

Saturation Effects. To evaluate aging and concentration effects, reaction mixtures were allowed to age and slowly evaporate until crystallization. The crystals were recovered and characterized (see above). Subsequently, saturated solutions were transferred into NMR tubes, and ^{31}P NMR spectra were collected (Figure 8). Quantification of the results obtained from these ^{31}P NMR spectra is not possible due to the variable quantities of crystalline products formed, including species containing non-stoichiometric amounts of U/Pp (e.g., $\{U_{24}\}\cdot\{U_{24}Pp_{12}\}$).

All saturated, crystal-yielding systems (pH = 4−10) gave NMR signals corresponding to $\{U_{24}Pp_{12}\}$ (δ = 3.80 ppm), an uncoordinated/small uranyl-peroxo pyrophosphate unit (δ = −3.50 to −7.18 ppm), and a pyrophosphate coordinated uranyl-peroxide tetramer, $\{U_4Pp_{4-x}\}$ (δ = −0.46 to −1.56 ppm). In addition to the signals observed under nonsaturated conditions, weak signals (~2% relative abundance) are observed, indicating the presence of the $\{U_{32}Pp_{16}\}$ anion at pH = 4−6 (Figure 8) suggesting that its formation is thermodynamically favored. The low abundance in solution and high crystal yields can be explained by low experimental solubility of $\{U_{32}Pp_{16}\}$ resulting in constant removal of the cluster from solution via crystallization followed by assembly of $\{U_{32}Pp_{16}\}$ from residual constituents present in the reaction mixture.

To validate our NMR peak assignments, a diffusion-ordered spectroscopy (DOSY) experiment was performed for the pH = 5 saturated solution, because this system provided the highest signal-to-noise ratio. In addition to measuring the viscosities and diffusion coefficients of the mother liquor (see Supporting Information), two standard solutions were prepared by dissolution of crystalline Li/Na salts of $\{U_{24}Pp_{12}\}$ and $\{U_{32}Pp_{16}\}$, and these provided hydrodynamic radii R_h of 14.89 ± 0.07 Å and 16.95 ± 0.28 Å, respectively (see Supporting Information). Each measured hydrodynamic radius exceeds the crystallographically determined value due to a solvation shell containing water molecules and alkali metal cations, as expected. The experimental values obtained for the reference materials follow the anticipated size trend ($R_h\{U_{24}Pp_{12}\} < R_h\{U_{32}Pp_{16}\}$), thereby providing evidence for each anion stability upon dissolution, and may be compared with the previously reported R_h value of 15.0 ± 0.1 Å for the $\{U_{24}Pp_{12}\}$.[32]

The ^{31}P DOSY NMR results obtained for the pH = 5 saturated solution are shown in Figure 9. The observed R_h value

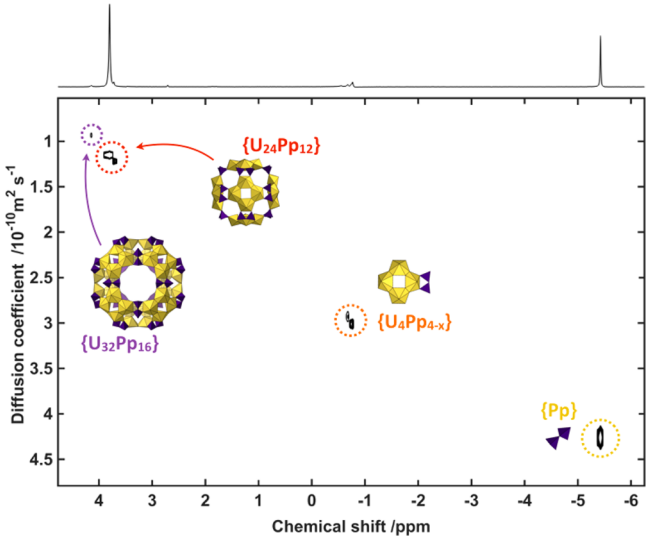

Figure 9. ^{31}P DOSY NMR spectra showing size-dependent diffusion coefficients obtained from saturated reaction mixture at pH = 5.

in conjunction with the NMR peak position and integrated intensity ratios indicate that the signals observed at 1.80/1.86 (d, $^2J_{P-P}$ = 13.5 Hz, R_h = N/A), 4.14 (s, R_h = 17.88 ± 0.67 Å), and 4.81/4.88 (d, $^2J_{P-P}$ = 13.5 Hz, R_h = N/A) are from intact $\{U_{32}Pp_{16}\}$. The signal at 3.80 ppm assigned to $\{U_{24}Pp_{12}\}$ yielded R_h = 13.69 ± 0.19 Å, confirming initial assignments. The differences in the observed R_h values obtained for $\{U_{24}Pp_{12}\}$ and $\{U_{32}Pp_{16}\}$ in ultrapure water and reaction mixtures arises from the dissimilar response of these anions to the constituents present in solution, resulting in slight variations of the associated solvation shell. The signals observed at −0.84 and −5.66 ppm provided an R_h of 5.57 ± 0.06 and 4.02 ± 0.05 Å, respectively. We assign the −0.84 ppm signal to $\{U_4Pp_{4-x}\}$ on the basis of the observed R_h value, the predicted size of this species, and results obtained from ^{31}P NMR and SAXS measurements of pH = 4 solution. Specifically, the Guinier analysis of the scattering curves obtained for this system provided an R_g value of 3.86 ± 0.06 Å, which paired with the anticipated size range for $\{U_4Pp_{4-x}\}$ (3.91−5.13 Å), and ^{31}P NMR measurement was assigned to the species observed at −0.84 ppm. Lastly, the signal observed at −5.66

DOI: 10.1021/acs.inorgchem.7b00649
Inorg. Chem. 2017, 56, 5478−5487

ppm (R_h = 4.02 ± 0.05 Å) is assigned to the uncoordinated pyrophosphate/small uranyl-peroxide pyrophosphate unit.

Amphoteric Nature of Uranyl Peroxides. The results presented herein demonstrate retention of basic uranyl peroxide building units such as {U_4} from the earliest stages of the reaction, followed by their pH-dependent assembly/disassembly. These moieties exhibit a unique amphoteric nature, as under alkaline conditions they condense to form uranyl peroxide nanoclusters (e.g., {U_{24}}),[23] then, provided the right chelating agents and a source of protons, disassemble into the original constituents and condense via an acid-promoted mechanism into functionalized uranyl peroxide nanoclusters (e.g., {$U_{24}Pp_{12}$}).[25] Because of the nature of their one-pot synthesis many uranyl peroxide nanoclusters have been assumed to form through a rather straightforward process where the constituents present in solution rapidly self-assemble to yield the final product.[24,29,54,57] Results obtained herein suggest that, in certain systems, formation of these nanostructures follows a well-defined reaction pathway consisting of multiple assembly/disassembly steps characterized by retention of the originally formed cyclic uranyl peroxide units. Figure 10 summarizes the generalized, acid-promoted reaction pathway for the formation of {$U_{32}Pp_{16}$} starting under alkaline conditions and in situ preassembled {U_{24}}.

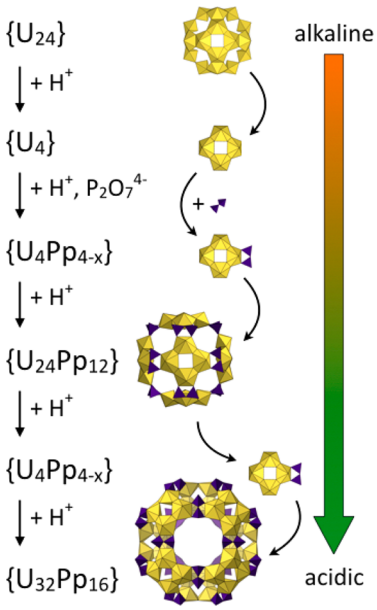

Figure 10. Schematic of the generalized acid-promoted formation of the {$U_{32}Pp_{16}$} anion.

CONCLUSIONS

The information obtained from systems containing stoichiometric amounts of uranium and pyrophosphate spanning a range of pH conditions provided insights into the mechanisms of uranyl peroxide nanocluster self-assembly. Formation of a novel binary {U_{24}}·{$U_{24}Pp_{12}$} cluster system under alkaline conditions provided evidence for the coexistence of different cluster species in solution and demonstrated that the Pp bridges undergo conformational changes upon crystallization. Acid-promoted formation of {$U_{24}Pp_{12}$}, followed by its dissociation and reassembly into {$U_{32}Pp_{16}$}, provides an example of hierarchical cluster synthesis requiring formation of a sacrificial cluster, whose components are scavenged to assemble a final product. The topological consistency observed across the range of studied pH values suggests the relative persistent character of the initially formed uranyl peroxide building blocks and highlights their amphoteric nature, allowing for assembly of clusters both in alkaline as well as acidic media. This study represents an important step toward controllable synthesis of task-specific uranyl peroxide nanoclusters.

ASSOCIATED CONTENT

Supporting Information

The Supporting Information is available free of charge on the ACS Publications website at DOI: 10.1021/acs.inorgchem.7b00649.

Variation of pH, ellipticity, crystallographic data, solvent-accessible void-space calculations, Raman spectroscopy, ESI-MS data, TGA data, ICP-OES data, SAXS, NMR data and discussion, additional references (PDF)

X-ray crystallographic information (CIF)

AUTHOR INFORMATION

Corresponding Author

*E-mail: pburns@nd.edu.

ORCID

William H. Casey: 0000-0002-3275-6465

Peter C. Burns: 0000-0002-2319-9628

Notes

The authors declare no competing financial interest.

ACKNOWLEDGMENTS

This material is based upon work supported as a part of the Materials Science of Actinides Center, and Energy Frontier Research Center funded by the U.S. Department of Energy, Office of Science, Office of Basic Energy Sciences, under Award No. DE-SC0001089. Traditional 1D ^{31}P NMR measurements were conducted at the Magnetic Resonance Research Center at the Univ. of Notre Dame. ^{31}P diffusion-ordered spectroscopy NMR measurements were conducted at the Nuclear Magnetic Resonance Facility at UC Davis. Raman spectroscopy and thermogravimetric analysis measurements were conducted at the Materials Characterization Facility of the Center for Sustainable Energy at the Univ. of Notre Dame. Electrospray ionization mass spectroscopy measurements were conducted at the Mass Spectrometry and Proteomics Facility at the Univ. of Notre Dame.

REFERENCES

(1) Ma, H. Y.; Peng, J.; Han, Z. G.; Yu, X.; Dong, B. X. A novel biological active multilayer film based on polyoxometalate with pendant support-ligand. *J. Solid State Chem.* **2005**, *178*, 3735−3739.

(2) Luong, T. K.; Shestakova, P.; Absillis, G.; Parac-Vogt, T. N. Detailed Mechanism of Phosphoanhydride Bond Hydrolysis Promoted by a Binuclear Zr^{IV}-Substituted Keggin Polyoxometalate Elucidated by a Combination of ^{31}P, ^{31}P DOSY, and ^{31}P EXSY NMR Spectroscopy. *Inorg. Chem.* **2016**, *55*, 4864−4873.

(3) Dianat, S.; Bordbar, A. K.; Tangestaninejad, S.; Zarkesh-Esfahani, S. H.; Habibi, P.; Abbasi Kajani, A. ctDNA interaction of Co-containing Keggin polyoxomolybdate and in vitro antitumor activity of free and its nano-encapsulated derivatives. *J. Iran. Chem. Soc.* **2016**, *13*, 1895−1904.

(4) Huang, Y. B.; Liang, J.; Wang, X. S.; Cao, R. Multifunctional metal-organic framework catalysts: synergistic catalysis and tandem reactions. *Chem. Soc. Rev.* **2017**, *46*, 126−157.

DOI: 10.1021/acs.inorgchem.7b00649
Inorg. Chem. 2017, 56, 5478−5487

(5) Muller, A.; Krickemeyer, E.; Bogge, H.; Schmidtmann, M.; Peters, F. Organizational forms of matter: An inorganic super fullerene and keplerate based on molybdenum oxide. *Angew. Chem., Int. Ed.* **1998**, *37*, 3359−3363.
(6) Muller, A.; Das, S. K.; Fedin, V. P.; Krickemeyer, E.; Beugholt, C.; Bogge, H.; Schmidtmann, M.; Hauptfleisch, B. Rapid and simple isolation of the crystalline molybdenum-blue compounds with discrete and linked nanosized ring-shaped anions: $Na_{15}[(Mo^{VI}_{126}Mo^{V}_{28}O_{462}H_{14})(H_2O)_{70}]_{0.5}$ $[(Mo^{VI}_{124}Mo^{V}_{28}O_{457}H_{14})(H_2O)_{68}]_{0.5}$···ca. 400 H_2O and $Na_{22}[(Mo^{VI}_{118}Mo^{V}_{28}O_{442}H_{14})(H_2O)_{58}]$···ca. 250 H_2O. *Z. Anorg. Allg. Chem.* **1999**, *625*, 1187−1192.
(7) Muller, A.; Botar, B.; Das, S. K.; Bogge, H.; Schmidtmann, M.; Merca, A. On the complex hedgehog-shaped cluster species containing 368 Mo atoms: simple preparation method, new spectral details and information about the unique formation. *Polyhedron* **2004**, *23*, 2381−2385.
(8) Long, D. L.; Burkholder, E.; Cronin, L. Polyoxometalate clusters, nanostructures and materials: From self assembly to designer materials and devices. *Chem. Soc. Rev.* **2007**, *36*, 105−121.
(9) Sans, V.; Cronin, L. Towards dial-a-molecule by integrating continuous flow, analytics and self-optimization. *Chem. Soc. Rev.* **2016**, *45*, 2032−2043.
(10) Roy, S.; Sarkar, S.; Pan, J.; Waghmare, U. V.; Dhanya, R.; Narayana, C.; Peter, S. C. Crystal Structure and Band Gap Engineering in Polyoxometalate-Based Inorganic-Organic Hybrids. *Inorg. Chem.* **2016**, *55*, 3364−3377.
(11) Izzet, G.; Abecassis, B.; Brouri, D.; Piot, M.; Matt, B.; Serapian, S. A.; Bo, C.; Proust, A. Hierarchical Self-Assembly of Polyoxometalate-Based Hybrids Driven by Metal Coordination and Electrostatic Interactions: From Discrete Supramolecular Species to Dense Monodisperse Nanoparticles. *J. Am. Chem. Soc.* **2016**, *138*, 5093−5099.
(12) Dolbecq, A.; Dumas, E.; Mayer, C. R.; Mialane, P. Hybrid Organic-Inorganic Polyoxometalate Compounds: From Structural Diversity to Applications. *Chem. Rev.* **2010**, *110*, 6009−6048.
(13) Song, Y. F.; Tsunashima, R. Recent advances on polyoxometalate-based molecular and composite materials. *Chem. Soc. Rev.* **2012**, *41*, 7384−7402.
(14) Wylie, E. M.; Peruski, K. M.; Weidman, J. L.; Phillip, W. A.; Burns, P. C. Ultrafiltration of Uranyl Peroxide Nanoclusters for the Separation of Uranium from Aqueous Solution. *ACS Appl. Mater. Interfaces* **2014**, *6*, 473−479.
(15) Wylie, E. M.; Peruski, K. M.; Prizio, S. E.; Bridges, A. N. A.; Rudisill, T. S.; Hobbs, D. T.; Phillip, W. A.; Burns, P. C. Processing used nuclear fuel with nanoscale control of uranium and ultrafiltration. *J. Nucl. Mater.* **2016**, *473*, 125−130.
(16) Odoh, S. O.; Schreckenbach, G. DFT Study of Uranyl Peroxo Complexes with H_2O, F^-, OH^-, CO_3^{2-}, and NO_3^-. *Inorg. Chem.* **2013**, *52*, 5590−5602.
(17) Soto, C. A. T.; Carauta, A. N. M.; Carneiro, J. W. D. M. DFT studies of structure and vibrational frequencies of isotopically substituted Diamin uranyl nitrate using relativistic effective core potentials. *Spectrochim. Acta, Part A* **2008**, *71*, 1140−1145.
(18) Shundalau, M. B.; Zazhogin, A. A.; Zazhogin, A. P.; Komyak, A. I.; Umreiko, D. S. Structure and Vibrational Spectra of Uranyl Dinitrate Complexes with Water and DMSO. *J. Appl. Spectrosc.* **2015**, *82*, 25−32.
(19) Oda, Y.; Aoshima, A. Ab initio quantum chemical study on charge distribution and molecular structure of uranyl (VI) species with Raman frequency. *J. Nucl. Sci. Technol.* **2002**, *39*, 647−654.
(20) Garcia-Hernandez, M.; Willnauer, C.; Kruger, S.; Moskaleva, L. V.; Rosch, N. Systematic DFT study of gas phase and solvated uranyl and neptunyl complexes $[AnO_2X_4]^n$ (An = U, Np; X = F, Cl, OH, n = −2; X = H_2O, n = + 2). *Inorg. Chem.* **2006**, *45*, 1356−1366.
(21) Armstrong, C. R.; Nyman, M.; Shvareva, T.; Sigmon, G. E.; Burns, P. C.; Navrotsky, A. Uranyl peroxide enhanced nuclear fuel corrosion in seawater. *Proc. Natl. Acad. Sci. U. S. A.* **2012**, *109*, 1874−1877.
(22) Burns, P. C.; Ewing, R. C.; Navrotsky, A. Nuclear Fuel in a Reactor Accident. *Science* **2012**, *335*, 1184−1188.
(23) Burns, P. C.; Kubatko, K. A.; Sigmon, G.; Fryer, B. J.; Gagnon, J. E.; Antonio, M. R.; Soderholm, L. Actinyl peroxide nanospheres. *Angew. Chem., Int. Ed.* **2005**, *44*, 2135−2139.
(24) Qiu, J.; Burns, P. C. Clusters of Actinides with Oxide, Peroxide, or Hydroxide Bridges. *Chem. Rev.* **2013**, *113*, 1097−1120.
(25) Ling, J.; Qiu, J.; Sigmon, G. E.; Ward, M.; Szymanowski, J. E. S.; Burns, P. C. Uranium Pyrophosphate/Methylenediphosphonate Polyoxometalate Cage Clusters. *J. Am. Chem. Soc.* **2010**, *132*, 13395−13402.
(26) Vlaisavljevich, B.; Gagliardi, L.; Burns, P. C. Understanding the Structure and Formation of Uranyl Peroxide Nanoclusters by Quantum Chemical Calculations. *J. Am. Chem. Soc.* **2010**, *132*, 14503−14508.
(27) Dembowski, M.; Olds, T. A.; Pellegrini, K. L.; Hoffmann, C.; Wang, X. P.; Hickam, S.; He, J. H.; Oliver, A. G.; Burns, P. C. Solution ^{31}P NMR Study of the Acid-Catalyzed Formation of a Highly Charged $\{U_{24}Pp_{12}\}$ Nanocluster, $[(UO_2)_{24}(O_2)_{24}(P_2O_7)_{12}]^{48-}$, and Its Structural Characterization in the Solid State Using Single-Crystal Neutron Diffraction. *J. Am. Chem. Soc.* **2016**, *138*, 8547−8553.
(28) Qiu, J.; Dembowski, M.; Szymanowski, J. E. S.; Toh, W. C.; Burns, P. C. Time-Resolved X-ray Scattering and Raman Spectroscopic Studies of Formation of a Uranium-Vanadium-Phosphorus-Peroxide Cage Cluster. *Inorg. Chem.* **2016**, *55*, 7061−7067.
(29) Falaise, C.; Nyman, M. The Key Role of U_{28} in the Aqueous Self-Assembly of Uranyl Peroxide Nanocages. *Chem. - Eur. J.* **2016**, *22*, 14678−14687.
(30) Miro, P.; Vlaisavljevich, B.; Gil, A.; Burns, P. C.; Nyman, M.; Bo, C. Self-Assembly of Uranyl-Peroxide Nanocapsules in Basic Peroxidic Environments. *Chem. - Eur. J.* **2016**, *22*, 8571−8578.
(31) Levitt, M. H. *Spin Dynamics: Basics of Nuclear Magnetic Resonance;* Wiley: 2001.
(32) Johnson, R. L.; Ohlin, C. A.; Pellegrini, K.; Burns, P. C.; Casey, W. H. Dynamics of a Nanometer-Sized Uranyl Cluster in Solution. *Angew. Chem., Int. Ed.* **2013**, *52*, 7464−7467.
(33) Oliveri, A. F.; Pilgrim, C. D.; Qiu, J.; Colla, C. A.; Burns, P. C.; Casey, W. H. Dynamic Phosphonic Bridges in Aqueous Uranyl Clusters. *Eur. J. Inorg. Chem.* **2016**, *2016*, 797−801.
(34) Floquet, S.; Brun, S.; Lemonnier, J. F.; Henry, M.; Delsuc, M. A.; Prigent, Y.; Cadot, E.; Taulelle, F. Molecular weights of cyclic and hollow clusters measured by DOSY NMR spectroscopy. *J. Am. Chem. Soc.* **2009**, *131*, 17254−17259.
(35) Shestakova, P.; Absillis, G.; Martin-Martinez, F. J.; De Proft, F.; Willem, R.; Parac-Vogt, T. N. Integrating 31P DOSY NMR spectroscopy and molecular mechanics as a powerful tool for unraveling the chemical structures of polyoxomolybdate-based amphiphilic nanohybrids in aqueous solution. *Chem. - Eur. J.* **2014**, *20*, 5258−5270.
(36) Burns, P. C.; Hughes, K. A. Studtite, $[(UO_2)(O_2)(H_2O)_2](H_2O)_2$: The first structure of a peroxide mineral. *Am. Mineral.* **2003**, *88*, 1165−1168.
(37) Krause, L.; Herbst-Irmer, R.; Stalke, D. An empirical correction for the influence of low-energy contamination. *J. Appl. Crystallogr.* **2015**, *48*, 1907−1913.
(38) Sheldrick, G. M. Crystal structure refinement with SHELXL. *Acta Crystallogr., Sect. C: Struct. Chem.* **2015**, *71*, 3−8.
(39) Sheldrick, G. M. SHELXT - Integrated space-group and crystal-structure determination. *Acta Crystallogr., Sect. A: Found. Adv.* **2015**, *71*, 3−8.
(40) Ilavsky, J.; Jemian, P. R. Irena: tool suite for modeling and analysis of small-angle scattering. *J. Appl. Crystallogr.* **2009**, *42*, 347−353.
(41) Cohn, M.; Hughes, T. R. Phosphorus Magnetic Resonance Spectra of Adenosine Diphosphate and Triphosphate 0.1. Effect of Ph. *J. Biol. Chem.* **1960**, *235*, 3250−3253.
(42) Marschner, T. M.; Reynolds, M. A.; Oppenheimer, N. J.; Kenyon, G. L. Isotope-Induced Non-Equivalence in a Symmetrical

DOI: 10.1021/acs.inorgchem.7b00649
Inorg. Chem. 2017, 56, 5478−5487

Molecule - Measurement of the ^{31}P-^{31}P Geminal Coupling-Constant in Pyrophosphate. *J. Chem. Soc., Chem. Commun.* **1983**, *0*, 1289−1290.
(43) Alam, T. M.; Liao, Z. L.; Zakharov, L. N.; Nyman, M. Solid-State Dynamics of Uranyl Polyoxometalates. *Chem. - Eur. J.* **2014**, *20*, 8302−8307.
(44) Nyman, M.; Alam, T. M. Dynamics of Uranyl Peroxide Nanocapsules. *J. Am. Chem. Soc.* **2012**, *134*, 20131−20138.
(45) Yin, P. C.; Li, D.; Liu, T. B. Solution behaviors and self-assembly of polyoxometalates as models of macroions and amphiphilic polyoxometalate-organic hybrids as novel surfactants. *Chem. Soc. Rev.* **2012**, *41*, 7368−7383.
(46) Hou, Y.; Zakharov, L. N.; Nyman, M. Observing Assembly of Complex Inorganic Materials from Polyoxometalate Building Blocks. *J. Am. Chem. Soc.* **2013**, *135*, 16651−16657.
(47) Goberna-Ferron, S.; Park, D. H.; Amador, J. M.; Keszler, D. A.; Nyman, M. Amphoteric Aqueous Hafnium Cluster Chemistry. *Angew. Chem., Int. Ed.* **2016**, *55*, 6221−6224.
(48) Izzet, G.; Abecassis, B.; Brouri, D.; Piot, M.; Matt, B.; Serapian, S. A.; Bo, C.; Proust, A. Hierarchical Self-Assembly of Polyoxometalate-Based Hybrids Driven by Metal Coordination and Electrostatic Interactions: From Discrete Supramolecular Species to Dense Monodisperse Nanoparticles. *J. Am. Chem. Soc.* **2016**, *138*, 5093−5099.
(49) Yin, P.; Wu, B.; Li, T.; Bonnesen, P. V.; Hong, K. L.; Seifert, S.; Porcar, L.; Do, C.; Keum, J. K. Reduction-Triggered Self-Assembly of Nanoscale Molybdenum Oxide Molecular Clusters. *J. Am. Chem. Soc.* **2016**, *138*, 10623−10629.
(50) Svergun, D.; Barberato, C.; Koch, M. H. J. CRYSOL - A program to evaluate x-ray solution scattering of biological macromolecules from atomic coordinates. *J. Appl. Crystallogr.* **1995**, *28*, 768−773.
(51) Maki, H.; Tsujito, M.; Yamada, T. Intrinsic ^{31}P NMR Chemical Shifts and the Basicities of Phosphate Groups in a Short-Chain Imino Polyphosphate. *J. Solution Chem.* **2013**, *42*, 1063−1074.
(52) Miro, P.; Pierrefixe, S.; Gicquel, M.; Gil, A.; Bo, C. On the Origin of the Cation Templated Self-Assembly of Uranyl-Peroxide Nanoclusters. *J. Am. Chem. Soc.* **2010**, *132*, 17787−17794.
(53) Sigmon, G. E.; Weaver, B.; Kubatko, K. A.; Burns, P. C. Crown and Bowl-Shaped Clusters of Uranyl Polyhedra. *Inorg. Chem.* **2009**, *48*, 10907−10909.
(54) Sigmon, G. E.; Burns, P. C. Rapid Self-Assembly of Uranyl Polyhedra into Crown Clusters. *J. Am. Chem. Soc.* **2011**, *133*, 9137−9139.
(55) Liao, Z. L.; Deb, T.; Nyman, M. Elucidating Self-Assembly Mechanisms of Uranyl Peroxide Capsules from Monomers. *Inorg. Chem.* **2014**, *53*, 10506−10513.
(56) Qiu, J.; Ling, J.; Jouffret, L.; Thomas, R.; Szymanowski, J. E. S.; Burns, P. C. Water-soluble multi-cage super tetrahedral uranyl peroxide phosphate clusters. *Chem. Sci.* **2014**, *5*, 303−310.
(57) Ling, J.; Qiu, J.; Burns, P. C. Uranyl Peroxide Oxalate Cage and Core-Shell Clusters Containing 50 and 120 Uranyl Ions. *Inorg. Chem.* **2012**, *51*, 2403−2408.

DOI: 10.1021/acs.inorgchem.7b00649
Inorg. Chem. 2017, 56, 5478−5487